Lateral optical force on linearly polarized dipoles near a magneto-optical surface based on polarization conversion

J. A. Girón-Sedas ⊙

Departamento de Física, Universidad del Valle, AA 25360, Cali, Colombia

Jack J. Kingsley-Smith and Francisco J. Rodríguez-Fortuño[*]

Department of Physics and London Centre for Nanotechnology, King's College London, WC2R 2LS, United Kingdom

Novel lateral optical forces acting on dipoles near surfaces have been investigated in the past few years: circularly polarized dipoles experience lateral optical forces when in proximity to a surface due to the recoil of directionally excited modes. Recent work shows that even linearly polarized dipoles may experience lateral forces when nonreciprocal substrates are used, due to the asymmetric propagation of modes in the surface. We theoretically show that a linearly polarized particle emitting in close proximity to a magneto-optical substrate may experience a lateral optical force even if the external magnetic field is normal to the surface plane. The polarization conversion of the magneto-optic material introduces a gradient in the quasistatic fields reflected from the surface, resulting in a lateral optical force, and also gives surface plasmons a hybrid polarization character, which alters the surface plasmon directional excitation from the dipole, resulting in an optical recoil force. We envisage potential applications in nanomechanical devices, since similar magnetoplasmonic architectures have already been developed experimentally.

I. INTRODUCTION

Since the confirmation that electromagnetic waves carry momentum and angular momentum [1,2], the study of light-matter interactions has resulted in important scientific advances in laser cooling [3,4], optical manipulation of atoms/small particles [5–10], and in optomechanical systems [11]. Recently there has been enormous interest in optical phenomena where spin-orbit interactions of light enable a robust spin controlled unidirectional propagation of surface or waveguide modes [12–15]. In particular, when a dipolar particle is emitting circularly polarized light near a surface supporting electromagnetic modes, spin-orbit coupling allows unidirectional excitation of these modes which carry electromagnetic momentum, and generate a recoil force that pushes the particle back in the opposite direction [16–18]. Similar lateral forces can arise by the directional far-field emission of chiral particles in evanescent fields [19]. All these unusual lateral forces have significant consequences in the optical manipulation of chiral [17,19] and nonchiral nanoparticles [16,18], as well as playing an important role in lateral Casimir forces [20]. These forces form a promising path to the simultaneous movement, arrangement, and sorting of particles on an isotropic substrate or waveguide in a simple way without structured or focused illumination. In general, such lateral optical forces cannot appear when the dipoles are linearly polarized, since there is no mode directionality in that case, as long as reciprocity of the surface is assumed.

However, when the surface is nonreciprocal, for example in magnetized plasma and photonic topological insulators, the modes sustained at the interface may become unidirectional [21–24] and therefore, lateral recoil forces on nearby dipoles arise [25,26]. Previous works typically use a magnetic field oriented parallel to the interface to break reciprocity, as this naturally breaks rotational symmetry of the surface modes, enabling their propagation in only one direction. In that case, any dipolar source will necessarily excite light directionally, providing a recoil force in a lateral direction determined only by the direction of the magnetic field, and independent of the dipole's polarization. Another known method to achieve dipolar directional scattering near a surface is to consider the effect of combined electric and magnetic dipole contributions [27–32], which may also produce lateral forces [33]. However, in this work we will focus on electric dipoles only, but considering a magnetic bias in nearby surfaces.

In this paper we demonstrate that magneto-optical (MO) surfaces allow the existence of a lateral force acting on a linearly polarized dipolar particle, even in the case when the magnetization is in the direction normal to the surface, see Fig. 1. This is surprising because the modes supported by the surface are identical in every direction due to symmetry. The appearance of this force is a consequence of the polarization conversion on the surface reflection coefficients. We show that this novel lateral force has different components. One of the components of the lateral force arises because surface plasmon modes acquire a hybrid polarization character in the presence of the magnetization, changing from being purely p polarized, to being a hybrid combination of p and s polarization. As we will show, this enables directionality of evanescent

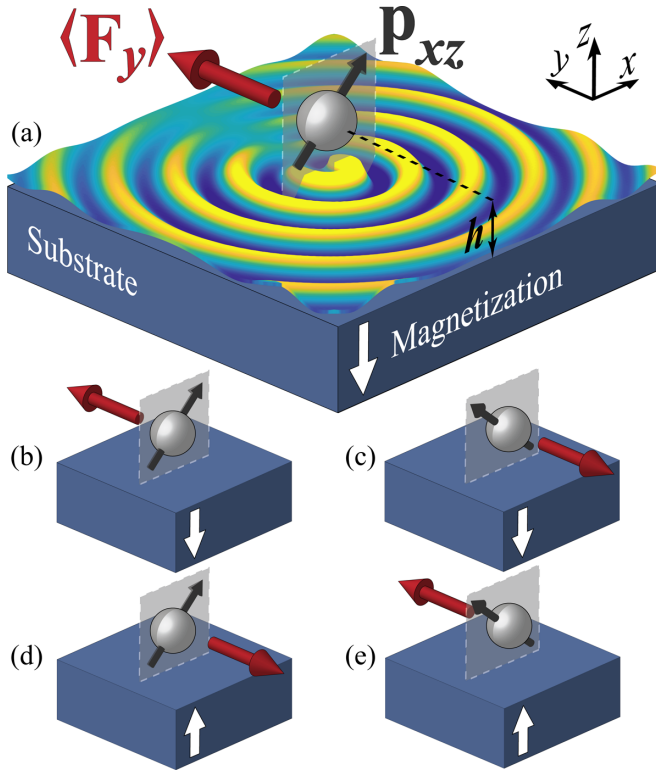*francisco.rodriguez_fortuno@kcl.ac.uk

FIG. 1. (a) Re$\{H_z\}$ emission of a linearly polarized dipole $\mathbf{p}_{xz}$ in the XZ plane over a magneto-optical surface. The conversion of polarization introduces a directionality of emission in the y direction, with a corresponding novel recoil optical force $\langle F_y \rangle$. (b)–(d) Diagrams depicting how the force switches direction when the degree of diagonal polarization χ and the magnetization $\mathbf{M}$ are inverted: (b) $\chi = +1$, $\mathbf{M} \propto -\mathbf{z}$. (c) $\chi = -1$, $\mathbf{M} \propto -\mathbf{z}$. (d) $\chi = +1$, $\mathbf{M} \propto +\mathbf{z}$. (e) $\chi = -1$, $\mathbf{M} \propto +\mathbf{z}$.

excitation of the modes from the dipole, inducing a recoil force on the particle. Magneto-optical (MO) surfaces could provide tunability to a nanomanipulation system through the modulation of the external magnetic field (and the corresponding magnetization) [34–38]. Our results were obtained analytically via the exact Green's function formalism of a dipole over a surface; using the dipole angular spectrum approach [33,39–42], together with the Fresnel reflection coefficients of the surface, in which the contribution of the magneto-optics has been included. Our results are confirmed with numerical simulations.

II. THEORETICAL FRAMEWORK

We consider an electric dipole source $\mathbf{p} = (p_x, 0, p_z)$ located in free space at $\mathbf{r}_0 = (0, 0, h)$ (Fig. 1). The dipole is radiating with an angular frequency ω above a semi-infinite magneto-optical substrate, which spans the region $z \leqslant 0$. The magnetization of this MO material is directed along the z axis, thus, the dielectric permittivity tensor may be written as $\varepsilon_{xx} = \varepsilon_{yy} = \varepsilon_{zz} = \varepsilon_2$ for the diagonal elements, and $\varepsilon_{xy} = -\varepsilon_{yx}$ for the off-diagonal ones [35]. The time-averaged optical force $\langle \mathbf{F} \rangle$ acting on the dipole can be deduced from the Lorentz electromagnetic force acting on the oscillating charges of a dipole due to the backscattered fields from the surface, and is

given by [41,43,44]

$$\langle \mathbf{F} \rangle = \sum_{i=x,y,z} \frac{1}{2} \mathrm{Re}\{p_i^* \nabla E_i\}, \tag{1}$$

where ∇ is the gradient with respect to $\mathbf{r}$ evaluated at $\mathbf{r}_0$, and $\mathbf{E} = (E_x, E_y, E_z)$ is the field reflected by the surface, acting back on the dipole, which may be calculated following the usual Green's function approach (see Appendix A). Since the aim of this work is to study the lateral forces (perpendicular to the z axis) acting on the dipole, we will focus on the y component of the force when the particle is diagonally polarized on the xz plane. The most general case of arbitrary dipole polarizations and force components is given in Appendix B, but all novel physics can be distilled into the specific scenario considered here. After substituting the reflected fields into Eq. (1), we arrive at the following compact, exact results:

$$\langle F_y \rangle = -\frac{3}{4c_0} P_{\mathrm{rad}}^{xz} \chi$$
$$\times \mathrm{Re}\left\{ \int_0^\infty r_{pp} e^{4i\pi\left(\frac{h}{\lambda}\right)\sqrt{1-k_{\mathrm{tr}}^2}} k_{\mathrm{tr}}^3 \frac{\Phi_K}{\sqrt{1-k_{\mathrm{tr}}^2}} dk_{\mathrm{tr}} \right\}, \tag{2}$$

where the integration is performed over the normalized transverse wave vector $k_{\mathrm{tr}} = \frac{k_t}{k_0}$. $P_{\mathrm{rad}}^{xz} = \frac{\omega^4(|p_x|^2+|p_z|^2)}{12\pi\varepsilon_0 c_0^3}$ is the power radiated by the x and z components of the dipole if it was placed in free space, λ is the wavelength, and $\chi = \frac{2\,\mathrm{Re}[p_x^* p_z]}{|p_x|^2+|p_z|^2}$ is a measure of the degree of diagonal polarization of the dipole; it is equal to 0 when the dipole is circularly polarized, or is horizontally or vertically polarized with respect to the surface, and is equal to ± 1 when the dipole is linearly polarized at 45 deg to the surface, where the $\pm$ sign accounts for a tilt towards or away from the x axis. The term $\Phi_K = r_{ps}/r_{pp}$ is the MO Kerr effect, where r_{pp}, r_{ss}, and r_{ps} are the Fresnel reflection coefficients for p polarization, s polarization, and s-to-p polarization conversion, respectively, and they all depend on the transverse wave-vector k_t and angular frequency ω (see Appendix C).

We may also obtain an approximate closed expression for the force in the near-field quasistatic approximation (see Appendix D), which applies when the dipole is very close to the surface. In this case, the force is given approximately by

$$\langle F_y^{\mathrm{QS}} \rangle \approx \left(\frac{3}{128\, c_0\, \pi^2} \right) P_{\mathrm{rad}}^{xz} \chi\, \mathrm{Re}\left\{ \frac{\varepsilon_{xy}}{1+\varepsilon_2} \right\} \left(\frac{h}{\lambda} \right)^{-2}. \tag{3}$$

This expression provides clear insight into the behavior of this force. It shows its dependence on the dipole polarization χ, being maximum in magnitude for diagonally polarized dipoles, and that the direction of the force (sign on χ) can be switched by changing the direction of the tilt of the linear polarization [see Figs. 1(b)–1(e)]. Equation (3) also shows the dependence on the off-diagonal permittivity ε_{xy}, whose sign flips when changing the orientation of the substrate magnetization, as shown in Figs. 1(b)–1(e). Finally, we see the dependence of the force when the distance to the surface is $\left(\frac{h}{\lambda} \right)^{-2}$, which is an unusually long range for a quasistatic scenario. For example, the known recoil forces from circularly polarized dipoles decay as $\left(\frac{h}{\lambda} \right)^{-4}$ in the quasistatic approximation [16].

The quasistatic approximation in Eq. (3) is one of the terms into which Eq. (2) can be decomposed, and it always dominates when $h \to 0$. However, we can use the same arguments used in Ref. [16] to decompose Eq. (2) into other terms, each dominant at a different range of distances h between the dipole and the surface (see Appendix E for an explicit form of each term and their range of validity). When the dipole height is in the reactive near-field region (typically considered as $h < \lambda/4\pi$) we can neglect the contribution to the force due to reflected propagating plane waves. In that near-field regime, the lateral force on the dipole can either be dominated by the quasistatic force [Eq. (3)], which can be thought of as the force exerted on the dipole by the image dipole formed at the surface [16,45], or by a mode-recoil force, caused by the directional excitation of any existing modes in the surface, resulting in an imbalance of linear momentum and an associated recoil mechanical force [16].

III. RESULTS AND DISCUSSION

Let us consider a realistic material as our magneto-optical surface. We will model a cobalt-silver alloy (Co_6Ag_{94}) at room temperature after annealing at $250\,^\circ C$ in the presence of an external magnetic field of 0.8 T. We will take a dipole radiation wavelength of $\lambda = 631$ nm such that the response of the diagonal and nondiagonal elements of the permittivity tensor is $\varepsilon_2 = -10.51 + 2.10i$ and $\varepsilon_{xy} = -1.2 + 1.15i$, respectively [46,47]. In order to appreciate the effect of the magnetization, we will also consider a non-magneto-optical substrate by keeping the same ε_2 as the magnetized Co_6Ag_{94} but setting $\varepsilon_{xy} = 0$.

In Figs. 2(a) and 2(b) we plot different electromagnetic field components at the substrate's surface, when a diagonally polarized dipole $\mathbf{p} = (1, 0, 1)$ is radiating above the non-magneto-optical metal substrate. The fields were calculated semianalytically following a Green function approach as described in Appendix A, but also independently confirmed via electromagnetic simulations in Comsol Multiphysics. In Fig. 2(a) a p-polarized surface plasmon mode is observed, propagating away from the source, having equal strength in any two diametrically opposite directions, which eliminates the possibility of the existence of a net lateral recoil optical force contribution. Figure 2(b) shows the H_z component of the magnetic field. This figure does not show any surface wave, because p-polarized modes—which are the only modes supported by this plasmonic surface—do not carry this magnetic field component, which would only exist in s-polarized modes. Instead, Fig. 2(b) is showing the near-field reflected fields, corresponding to the image dipole. In this case, the image dipole fields are symmetric and no lateral gradient is established, hence there is no quasistatic contribution to the lateral force either. The net lateral force is therefore zero, as it corresponds to a linearly polarized dipole near a reciprocal surface.

The application of a static magnetic field on the system along the z axis (or if the substrate itself shows a spontaneous magnetization) breaks the time reversal symmetry as well as Lorentz reciprocity, inducing the appearance of off-diagonal terms in the dielectric permittivity tensor ε_{xy}. This class of materials, called MO materials, allow electromagnetic
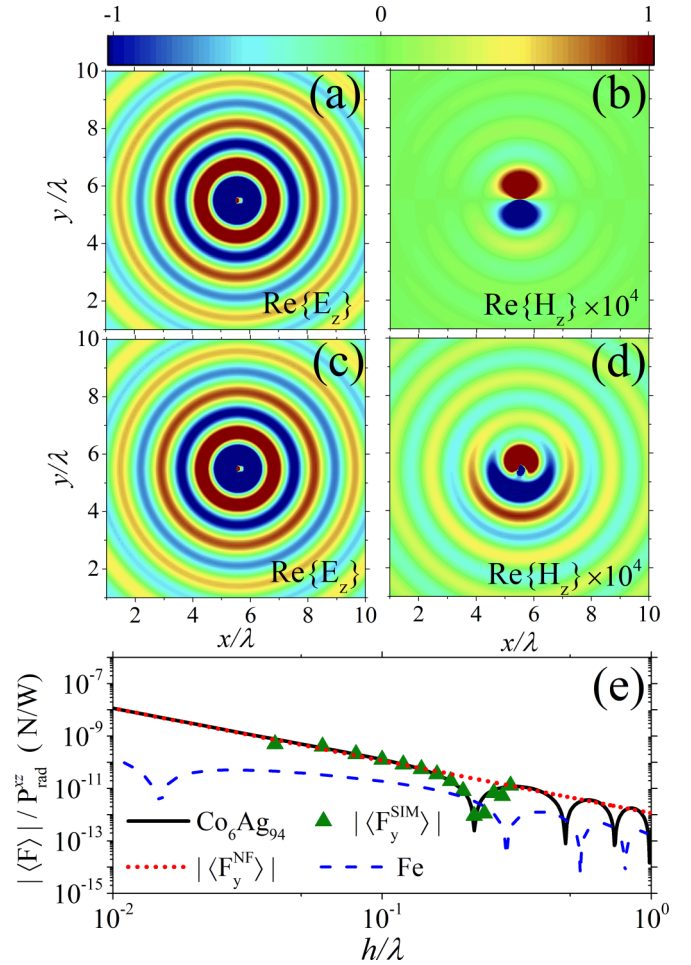

FIG. 2. Magnetic field distribution induced by a linearly polarized dipole $\mathbf{p} = (1, 0, 1)$, located at $h = 0.018\lambda$ ($\lambda = 632.8$ nm) above (a) and (b): a metallic surface ($\varepsilon_2 = -10.51 + 2.10i$) and (c) and (d) a realistic magneto-optical surface (diagonal $\varepsilon_2 = -10.51 + 2.10i$ and off-diagonal $\varepsilon_{xy} = -1.20 + 1.15i$ element of the permittivity tensor). (e) Distance dependence of the time-averaged lateral forces over a MO metal Co_6Ag_{94} (solid line) and iron (dashed line) substrate. The conversion of polarization allows the existence of $\langle F_y \rangle$ (solid and dashed lines), which matches well to the near-field approximation $\langle F_y^{QS} \rangle$ (dotted lines) when the dipole is close to the surface. The triangles correspond to the numerically simulated force $\langle F_y^{SIM} \rangle$ at different heights using Maxwell's stress tensor in a COMSOL Multiphysics simulation.

waves to propagate as elliptically polarized waves through them with different speeds. This leads to a rotation of the polarization plane of both transmitted and reflected fields at their interface [35,38]. This also leads to a modification in the polarization of the surface plasmon modes which exist at the interface: instead of being purely p polarized, they acquire a hybrid character, becoming a fixed superposition of p and s polarization (see Appendix E). This can have an effect on the directionality of excitation of modes by the dipole, however, in this realistic case the effect is very small. In Figs. 2(c) and 2(d) we study the same metallic surface analyzed in Figs. 2(a) and 2(b) but adding a magneto-optical response, corresponding to the dielectric permittivity tensor of Co_6Ag_{94} mentioned above, characterized by the presence of

off-diagonal elements ε_{xy}. From Eq. (2), we know that this will imply the appearance of a lateral force $\langle F_y \rangle$ which depends strongly on the polarization conversion of the reflected fields Φ_K when the system shows a MO response. By looking at the fields, we can understand whether the force comes from the quasistatic or the mode recoil contributions. Figure 2(c) shows the surface plasmon, seemingly identical to the non-MO case in Fig. 2(a). A quantitative study of the fields, however, reveals that the surface plasmon (SPP) directionality in this case has a top/down ratio of 1.035:1, slightly directional, but not visible on this figure. Indeed, the lateral force contribution from surface plasmon recoil is negligible. The appearance of an s-polarized H_z field component of the surface plasmons is visible in the background of Fig. 2(d), as faint concentric circles that follow the same pattern as E_z in Fig. 2(c). Much more interesting is the central part of Fig. 2(d), showing how the quasistatic near fields have been modified and now exhibit a very clear lateral gradient in the y direction. This gradient is responsible for the quasistatic contribution to the lateral force, given in Eq. (3).

In order to estimate the strength of this force in realistic materials, we provide in Fig. 2(e) the dependence of the time-averaged force $\langle F_y \rangle$, normalized to the power radiated by the dipole, with respect to the distance h between the dipole and the surface. The graph corresponds to a linearly polarized dipole radiating over two examples of MO surfaces. The first one corresponds to the cobalt-silver alloy mentioned above. As expected, the force $\langle F_y \rangle$ is most intense when the dipole is very close to the substrate. In the reactive near-field region, at very subwavelength distances ($h < \lambda/4\pi$), we see that the exact result obtained for the cobalt-silver alloy using Eq. (2) agrees very well with the near-field quasistatic approximation from Eq. (3) (red dotted line). Beyond this distance, the force can be seen to change sign periodically. This is because the force becomes dominated by the phase-sensitive far-field plane wave force contribution (see Appendix E). The mode recoil contribution of the force, which would reveal itself as a lateral force decaying exponentially with the distance of the dipole to the surface, is not seen for the cobalt-silver alloy, because this component is negligible compared to the quasistatic contribution to the force. The figure also shows the calculation of the force from numerical simulations using the software COMSOL Multiphysics and Maxwell stress tensor integration, fully confirming our analytical derivations (triangles). The lateral force can be controlled via the polarization of the dipole and via the magnetization (see Fig. 1). For instance, the force changes sign if we use a dipole $\mathbf{p} = (-1, 0, 1)$.

The second example of realistic material shown in Fig. 2(e) is an iron substrate in the presence of an external magnetic field of 1.1 T (dashed line), whose dielectric permittivity tensor may be written as $\varepsilon_2 = -0.88 + 17.94i$ and $\varepsilon_{xy} = -0.67 + 0.09i$ when the dipole radiates at 632.8 nm [48–50]. For this material, in the reactive near-field region ($h < \lambda/4\pi$), we notice that the force has a change in sign (seen as a downwards peak in this logarithmic plot near $h/\lambda = 10^{-2}$). This is because the quasistatic component of the lateral force is opposed to the mode recoil force, so at a certain distance, the quasistatic component of the force becomes weak enough to be exactly canceled out by the mode recoil force. Above this distance, and up to $h \approx \lambda/2\pi$, the lateral force is dominated

by the plasmon recoil force term, whose origin we explain in depth later. Both examples illustrate the wide applicability of such lateral force and the possibility of an additional control to manipulation of particles over MO surfaces.

We have given an analytical prediction and numerical confirmation of the existence of this lateral force over a realistic surface in which the quasistatic term of the force dominates. However, the lateral force can also arise from a directionality in the excitation of surface plasmon modes by the diagonal dipole, enabled by the MO effect, as shown by the realistic iron substrate. To explain the physical origin of this directionality in mode excitation, we put forward a simplified model that is best illustrated by considering ideal lossless materials with relatively large off-diagonal components in the permittivity tensor. In the absence of MO effects, the electric field of a surface plasmon mode in a smooth interface is given by $\mathbf{E}_{SPP} \propto \hat{\mathbf{e}}_p^+$, where $\hat{\mathbf{e}}_p^+(\phi) = (i\sqrt{n_{SPP}^2 - 1} \cos\phi, i\sqrt{n_{SPP}^2 - 1} \sin\phi, -n_{SPP})$ is the basis vector corresponding to p polarization (see Appendix A) applied to a surface plasmon with effective index n_{SPP} propagating at a polar angle ϕ on the xy plane. In the presence of MO effects, the plasmon modes become hybrid $\mathbf{E}_{SPP} \propto (\hat{\mathbf{e}}_p^+ + \alpha\, \hat{\mathbf{e}}_s)$, where $\hat{\mathbf{e}}_s(\phi) = (-\sin\phi, \cos\phi, 0)$ is the basis unit vector corresponding to s polarization, and α is the fixed ratio between the p- and s-polarized components which characterizes the hybrid nature of the mode. The surface and the applied magnetic field are rotationally symmetric around the z axis, so the surface plasmon propagation constant and mode structure is identical in every direction due to symmetry. The value of α depends on the material and increases with the off-diagonal permittivity component (see Appendix F). The amplitude and phase with which this surface plasmon is excited by a dipolar source $\mathbf{p} = (p_x, 0, p_z)$ is given by Fermi's golden rule $\mathbf{p}^* \cdot \mathbf{E}_{SPP}$ [51–57], which after substitution of the plasmon fields yields

$$\mathbf{p}^* \cdot \mathbf{E}_{SPP}(\phi) \propto p_x^* \left[i \cos\phi \sqrt{n_{SPP}^2 - 1} - \alpha \sin\phi \right] - p_z^* n_{SPP}. \tag{4}$$

Equation (4) defines the planar radiation diagram of the surface modes excited by the dipole in every direction ϕ within the plane, as shown in Figs. 3(a)–3(d). For example, if we take $\phi = \{0, \pi\}$, which corresponds to a direction $\pm x$, the coupling amplitude is $\mathbf{p}^* \cdot \mathbf{E}_{SPP} \propto \pm p_x^* i\sqrt{n_{SPP}^2 - 1} - p_z^* n_{SPP}$. This translates into the well-known result that an elliptically polarized dipole $\mathbf{p} = (n_{SPP}, 0, i\sqrt{n_{SPP}^2 - 1})$ will achieve perfect directionality along $\pm x$. However, if we take $\phi = \{\frac{\pi}{2}, \frac{3\pi}{2}\}$, corresponding to excitation of surface modes in the $\pm y$ direction, the coupling amplitude is given by $\mathbf{p}^* \cdot \mathbf{E}_{SPP} \propto \mp p_x^* \alpha - p_z^* n_{SPP}$. This equation is key to understanding the novel mode-recoil component of the lateral optical force along y. First notice that with no MO effects $\alpha = 0$, only the p_z component will excite surface plasmons along $\pm y$, and it will do so with equal strength on both directions, hence resulting in no net recoil force along y. However, the presence of the additional s-polarized component of the hybrid modes in the MO substrate enables p_x to also contribute to the excitation of plasmons in the $\pm y$ direction. The coherent superposition of both excitations may result in near-field destructive
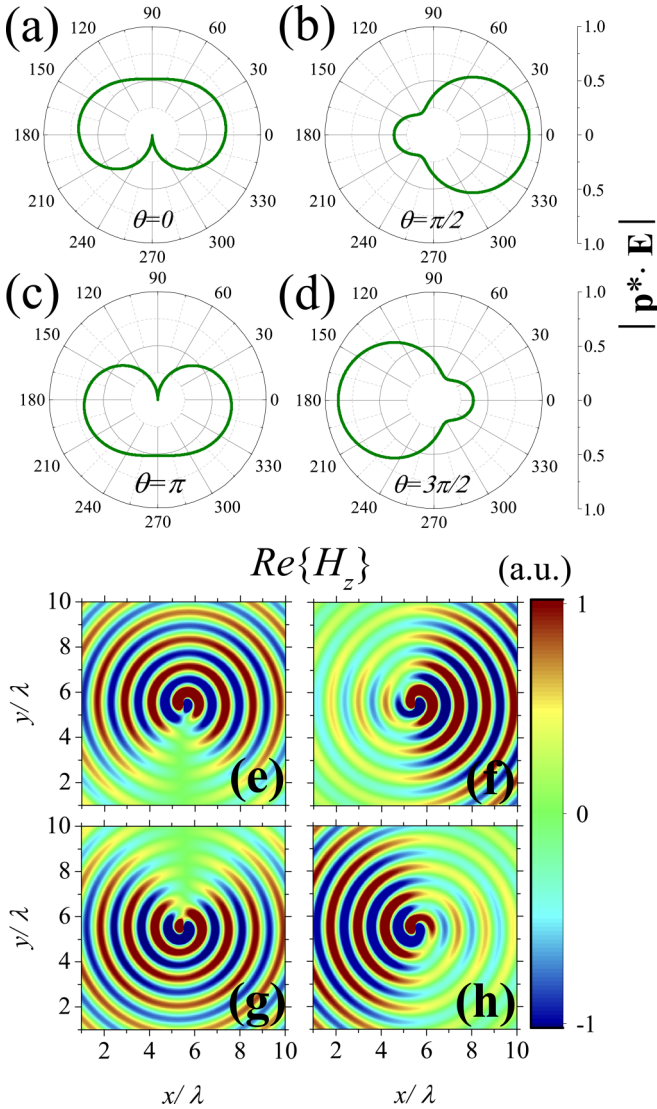
FIG. 3. (a)–(d) Planar radiation diagrams of the surface modes excited for different dipole polarizations. The polarization has been chosen as $p_z = \frac{1}{4} p_x e^{i\theta}$, where θ is the relative phase between p_z and p_x varied throughout as (a) $\theta = 0$, (b) $\theta = \frac{\pi}{2}$, (c) $\theta = \pi$, and (d) $\theta = \frac{3\pi}{2}$. The dipole polarization has been optimized according to $|p_x| = |p_z| n_{SPP}/\alpha$, to achieve maximum unidirectionality along the y axis. (e)–(h) Magnetic field distribution over the MO surface, confirming the unidirectionality reported in the radiation diagrams (a)–(d). Here the dipole is located at $h = 0.01\lambda$ above a toy model MO material ($\varepsilon_2 = -6 + 0.01i$ and $\varepsilon_{xy} = 6i$) for $\lambda = 500$ nm.

interference. The plasmons excited by p_z can destructively interfere with those excited by p_x in the $+y$ or $-y$ direction. This dual excitation is only possible thanks to the hybrid nature of the surface modes, enabled by the magneto-optics. The imbalance in excitation along the y axis must result in a corresponding recoil force in the opposite direction. For example, a maximum contrast of excitation is obtained when $p_x = \frac{p_z n_{SPP}}{\alpha}$. This optimized situation is shown in Figs. 3(a), 3(c), 3(e), and 3(g).

For lossless MO materials, α is a purely real value, and so the dipoles which achieve directionality along $\pm y$ are linearly polarized, tilted in the xz plane. This is very different to

the well-known directionality of circular dipoles along $\pm x$ which requires quadrature phase difference between p_x and p_z. Therefore, varying the phase difference between p_x and p_z (changing the polarization of the dipole from linear to elliptical) changes the directionality of excited plasmons in the xy plane, as shown in the panels of Fig. 3. This suggests the possibility of a tunable lateral force whose direction can be selected to point anywhere within the xy plane in an experimentally convenient way, by simply changing the polarization of illumination of a dipolar scatterer. This can be done easily, with no need for changes in the direction of incidence, hence, a single wide-area plane wave illumination could be used. This requires only electric dipoles and an MO surface. A similar tunable directionality effect was recently achieved experimentally without MO surface, but requiring the combination of electric and magnetic dipoles [58].

It might appear counterintuitive that the lateral optical force, as given by Eq. (2), is always maximum when the dipole is exactly diagonally polarized $p_x = p_z$, whereas the condition for maximum contrast in directionality occurs when $p_x = \frac{p_z n_{SPP}}{\alpha}$, as derived from Eq. (4) and used in Figs. 3(a), 3(c) 3(e), and 3(g). This apparent contradiction can be explained by noting that the magnitude of the recoil force is proportional to the *imbalance* in the net electromagnetic momentum, and not by its *contrast*. The net linear momentum vector of all the surface plasmons $\mathcal{P}$ propagating on the surface can be obtained via the angular integration of the linear momentum vectors of the individual surface plasmon waves propagating in each direction, which are proportional to the mode intensity and directed in the radial direction:

$$\mathcal{P} = \begin{pmatrix} \mathcal{P}_x \\ \mathcal{P}_y \\ 0 \end{pmatrix} \propto \int_0^{2\pi} \hat{\mathbf{e}}_r |\mathbf{p}^* \cdot \mathbf{E}_{SPP}|^2 d\phi, \tag{5}$$

where $\hat{\mathbf{e}}_r = (\cos\phi, \sin\phi, 0)$ is the unit vector in the radial direction. After substituting Eq. (4) into Eq. (5), we may analytically evaluate the integral in the lossless case (see Appendix G for the general case):

$$\begin{pmatrix} \mathcal{P}_x \\ \mathcal{P}_y \end{pmatrix} \propto 2\pi n_{SPP} \begin{pmatrix} \mathrm{Im}[p_x p_z^*]\sqrt{n_{SPP}^2 - 1} \\ \mathrm{Re}[p_x p_z^*]\alpha \end{pmatrix}. \tag{6}$$

This expression encompasses the existence of the usual lateral recoil force acting along x on circularly polarized dipoles, as well as the novel lateral force acting along y on linearly polarized dipoles, caused by the hybrid character of surface plasmons $\alpha \neq 0$ due to the MO effect. For a fixed dipole radiated power, the momentum imbalance in both the x and the y direction is greatest when $|p_x| = |p_z|$, corresponding to purely circular or purely diagonal polarization, respectively, in agreement with the calculation of the force.

IV. CONCLUSIONS

In conclusion, we have analytically and numerically demonstrated the existence, and have given a physical explanation, of an optical force acting on a dipole over a magneto-optical substrate with a magnetization perpendicular to the substrate, which emerges from the cross-polarized reflection of the surface. A comparison of the magnitude of this

force with previously known forces on a circularly polarized dipole is provided in Appendix H. Although we focused on surfaces with a magnetic bias, cross-polarization components may arise in other situations such as anisotropic surfaces [59], where this same force could appear. The existence of this force was not easy to predict for two reasons: (i) a linearly polarized dipole, even when diagonally polarized, does not provide near-field directionality of surface modes on its own when near a reciprocal substrate, and (ii) a MO material whose magnetization is normal to the surface also does not show an intrinsic directionality in the surface modes that it supports (unlike the more usual case of magnetization parallel to the surface). Both conditions are simultaneously needed. Indeed, symmetry considerations are subtle: The dipole tilt in the xz plane breaks the rotational symmetry around z while, by itself, would not break the mirror-reflection symmetry along mirror plane $y = 0$. On the other hand, the magnetization normal to the surface M_z, being a pseudovector, breaks the mirror-reflection symmetry along the mirror plane $y = 0$, while by itself it would not break the rotational symmetry around z. From symmetry considerations, *both* rotation and reflection symmetries need to be broken for a nonzero lateral force along y to arise. Indeed, when both are combined, such a force appears. Some previous works break the symmetry of surface modes via a magnetic field parallel to the surface, and therefore the direction of the force is independent of the polarization of the dipole. In this work, the dipole tilt is required for breaking the symmetry, and therefore the lateral force direction depends directly on, and therefore can be controlled by, the dipole polarization. This study suggests that nanosystems combining magnetic and plasmonic functionalities could prove strong candidates for the exploration and control of optical force technologies and applications.

APPENDIX A: DYADIC GREEN'S FUNCTION FOR A DIPOLE ABOVE SURFACE WITH CROSS-POLARIZED REFLECTION

Consider an arbitrary electric dipole **p** located at $\mathbf{r}_0 = (0, 0, h)$ within a homogeneous medium, as illustrated in Fig. 4. The total electric field is a solution of the wave equation and as such fulfils the corresponding dispersion relation for the wave-vector components $k_x^2 + k_y^2 + k_{z1}^2 = k_1^2$. Therefore, the electric field reaching the surface $\mathbf{E}_{inc}^{ED}$ generated by the dipole can be expressed using the angular spectrum representation [39–41] as

$$\mathbf{E}_{inc}^{ED}(x, y, z) = \iint \mathbf{E}_{inc}^{ED}(k_x, k_y)|_{z=h}^{\pm} e^{i(k_x x + k_y y \pm k_{z1}(z-h))} dk_x dk_y,$$
(A1)

where the integral is performed over $k_x, k_y \in [-\infty, \infty]$, $\mathbf{E}_{inc}^{ED}(k_x, k_y)|_{z=h}^{\pm}$ is the angular spectrum representation of the dipole fields at the plane $z = h$. The + and − sign are used
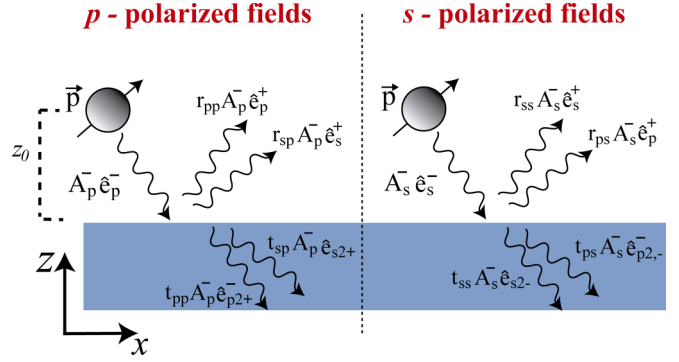

FIG. 4. Reflected fields by a surface with cross-polarized reflection.

to distinguish between fields radiated above and below the dipole $z = h$, respectively, corresponding to fields whose z dependence is $e^{\pm i k_{z1}(z-h)}$. The angular spectrum is a superposition of two polarization components: $\hat{\mathbf{e}}_s^{\pm}$ and $\hat{\mathbf{e}}_p^{\pm}$, which are the unit vectors of the electric field of s-polarized and p-polarized waves

$$\hat{\mathbf{e}}_s^{\pm} = \left(-\frac{k_y}{k_t}, \frac{k_x}{k_t}, 0 \right),$$
(A2)

$$\hat{\mathbf{e}}_p^{\pm} = \left(\pm \frac{k_x k_{z1}}{k_1 k_t}, \pm \frac{k_y k_{z1}}{k_1 k_t}, -\frac{k_t}{k_1} \right),$$
(A3)

where $k_t = \sqrt{k_x^2 + k_y^2}$, $k_1 = n_1 k_0$, n_1 is the refractive index of the medium, taken as free space in the main text, and $k_{z1} = \sqrt{k_1^2 - k_t^2}$, where we always take the sign of the square root that results in a positive imaginary part. Note that $\hat{\mathbf{e}}_s^{\pm}$ and $\hat{\mathbf{e}}_p^{\pm}$ correspond to the well-known unit vectors in spherical coordinates when describing propagating plane wave components inside the light cone ($k_x^2 + k_y^2 \leqslant k_1^2$), but can be extended with no alteration to their mathematical equation outside of the light cone, accurately describing the polarization of evanescent waves. Note that $\hat{\mathbf{e}}_s^{+} = \hat{\mathbf{e}}_s^{-}$ so it is unaffected by this sign and usually referred to as $\hat{\mathbf{e}}_s$. The angular spectrum of the field reaching the surface can be written as the sum of s- and p-polarized components:

$$\mathbf{E}_{inc}^{ED}(k_x, k_y)|_{z=0}^{-} = A_s^{-} \hat{\mathbf{e}}_s^{-} + A_p^{-} \hat{\mathbf{e}}_p^{-},$$
(A4)

where the amplitudes $A_{s,p}^{-}$ correspond to the angular spectrum of an electric dipole [42] propagated down to $z = 0$:

$$A_s^{-} = i \frac{k_1^2}{8\pi^2 \varepsilon_0 \varepsilon_1} \frac{1}{k_{z1}} e^{i k_{z1} h} (\hat{\mathbf{e}}_s^{-} \cdot \mathbf{p}),$$
(A5)

$$A_p^{-} = i \frac{k_1^2}{8\pi^2 \varepsilon_0 \varepsilon_1} \frac{1}{k_{z1}} e^{i k_{z1} h} (\hat{\mathbf{e}}_p^{-} \cdot \mathbf{p}).$$
(A6)

Since the surface is magneto-optic and its magnetization is along the z axis, the reflected and transmitted fields experience rotation of the polarization plane. Taking into account the polarization conversion, the reflected electric field reads

$$\mathbf{E}_{ref}^{ED}(k_x, k_y, z) = e^{i k_{z1} z} [r_{ss} A_s^{-} + r_{sp} A_p^{-}] \hat{\mathbf{e}}_s^{+}$$
$$+ e^{i k_{z1} z} [r_{ps} A_s^{-} + r_{pp} A_p^{-}] \hat{\mathbf{e}}_p^{+}, \quad (A7)$$

where the polarization vectors now have the $+$ superscript because they are propagating (or evanescently decaying) away from the surface in the $+z$ direction. Expanding the right-hand side of the above equation leads to

$$= i \frac{k_1^2}{8\pi^2\varepsilon_0\varepsilon_1} \frac{1}{k_{z1}} e^{ik_{z1}(h+z)} ([r_{ss}(\hat{\mathbf{e}}_s^- . \mathbf{p}) + r_{sp}(\hat{\mathbf{e}}_p^- . \mathbf{p})]\hat{\mathbf{e}}_s^+$$
$$+ [r_{ps}(\hat{\mathbf{e}}_s^- . \mathbf{p}) + r_{pp}(\hat{\mathbf{e}}_p^- . \mathbf{p})]\hat{\mathbf{e}}_p^+), \quad (A8)$$

and using the fact that $(\mathbf{a} \cdot \mathbf{p})\mathbf{b} = (\mathbf{b} \otimes \mathbf{a})\mathbf{p}$, we arrive at

$$= i \frac{k_1^2}{8\pi^2\varepsilon_0\varepsilon_1} \frac{1}{k_{z1}} e^{ik_{z1}(h+z)} [r_{ss}(\hat{\mathbf{e}}_s^+ \otimes \hat{\mathbf{e}}_s^-) + r_{sp}(\hat{\mathbf{e}}_s^+ \otimes \hat{\mathbf{e}}_p^-)$$
$$+ r_{ps}(\hat{\mathbf{e}}_p^+ \otimes \hat{\mathbf{e}}_s^-) + r_{pp}(\hat{\mathbf{e}}_p^+ \otimes \hat{\mathbf{e}}_p^-)]\mathbf{p}, \quad (A9)$$

where $\otimes$ represents an outer product. Performing the outer products, we have

$$\overleftrightarrow{\mathbf{M}}_{ss} = \frac{k_1^2}{k_{z1}} \hat{\mathbf{e}}_s \otimes \hat{\mathbf{e}}_s = \frac{k_1^2}{k_{z1}k_t^2} \begin{pmatrix} k_y^2 & -k_xk_y & 0 \\ -k_xk_y & k_x^2 & 0 \\ 0 & 0 & 0 \end{pmatrix}, \quad (A10)$$

$$\overleftrightarrow{\mathbf{M}}_{sp} = \frac{k_1^2}{k_{z1}} \hat{\mathbf{e}}_s \otimes \hat{\mathbf{e}}_p^- = \frac{k_1}{k_t^2} \begin{pmatrix} k_xk_y & k_y^2 & k_yk_t^2/k_{z1} \\ -k_x^2 & -k_xk_y & -k_xk_t^2/k_{z1} \\ 0 & 0 & 0 \end{pmatrix}, \quad (A11)$$

$$\overleftrightarrow{\mathbf{M}}_{ps} = \frac{k_1^2}{k_{z1}} \hat{\mathbf{e}}_p^+ \otimes \hat{\mathbf{e}}_s = \frac{k_1}{k_t^2} \begin{pmatrix} -k_xk_y & k_x^2 & 0 \\ -k_y^2 & k_xk_y & 0 \\ k_yk_t^2/k_{z1} & -k_xk_t^2/k_{z1} & 0 \end{pmatrix}, \quad (A12)$$

$$\overleftrightarrow{\mathbf{M}}_{pp} = \frac{k_1^2}{k_{z1}} \hat{\mathbf{e}}_p^+ \otimes \hat{\mathbf{e}}_p^-$$
$$= \begin{pmatrix} -k_{z1}k_x^2/k_t^2 & -k_{z1}k_xk_y/k_t^2 & -k_x \\ -k_{z1}k_xk_y/k_t^2 & -k_{z1}k_y^2/k_t^2 & -k_y \\ k_x & k_y & k_t^2/k_{z1} \end{pmatrix}. \quad (A13)$$

With the previous expressions (A10)–(A13), we can rewrite Eq. (A7) as follows:

$$\mathbf{E}_{\text{ref}}^{\text{ED}}(k_x, k_y, z) = \frac{i}{8\pi^2\varepsilon_0\varepsilon_1} e^{ik_{z1}(h+z)} \overleftrightarrow{\mathbf{M}} \mathbf{p}, \quad (A14)$$

where

$$\overleftrightarrow{\mathbf{M}} = r_{ss} \overleftrightarrow{\mathbf{M}}_{ss} + r_{sp} \overleftrightarrow{\mathbf{M}}_{sp} + r_{ps} \overleftrightarrow{\mathbf{M}}_{ps} + r_{pp} \overleftrightarrow{\mathbf{M}}_{pp}. \quad (A15)$$

Finally, the reflected electric field in real space is written as

$$\mathbf{E}_{\text{ref}}^{\text{ED}}(x, y, z) = \iint \mathbf{E}_{\text{ref}}^{\text{ED}}(k_x, k_y, z) \ e^{i(k_xx+k_yy)} dk_x dk_y. \quad (A16)$$

By substituting Eq. (A14) into Eq. (A16), and taking the constant dipole moment out of the integral, we finally arrive at the concept of the dyadic Green's function over the MO surface:

$$\mathbf{E}_{\text{ref}}^{\text{ED}}(\mathbf{r}) = \overleftrightarrow{\mathbf{G}}(\mathbf{r}, \mathbf{r}_0, \omega)\mathbf{p}, \quad (A17)$$

where

$$\overleftrightarrow{\mathbf{G}}(\mathbf{r}, \mathbf{r}_0, \omega) = \frac{i}{8\pi^2\varepsilon_0\varepsilon_1} \iint \overleftrightarrow{\mathbf{M}} e^{i(k_xx+k_yy+k_{z1}(h+z))} dk_x dk_y. \quad (A18)$$

For the calculation of the optical forces, we need the gradient of the fields. The gradient of Green's function with respect to $\mathbf{r} = (x, y, z)$ is given by

$$\nabla \overleftrightarrow{\mathbf{G}} = \frac{\partial \overleftrightarrow{\mathbf{G}}}{\partial x}\hat{\mathbf{x}} + \frac{\partial \overleftrightarrow{\mathbf{G}}}{\partial y}\hat{\mathbf{y}} + \frac{\partial \overleftrightarrow{\mathbf{G}}}{\partial z}\hat{\mathbf{z}}, \quad (A19)$$

where the spatial derivatives can be calculated from Eq. (A18) at the location of the dipole $\mathbf{r}_0 = (0, 0, h)$ as

$$\frac{\partial \overleftrightarrow{\mathbf{G}}}{\partial x}(\mathbf{r}_0, \mathbf{r}_0, \omega) = \frac{-1}{8\pi^2\varepsilon_0\varepsilon_1} \iint k_x \overleftrightarrow{\mathbf{M}} e^{i2k_{z1}h} dk_x dk_y, \quad (A20)$$

$$\frac{\partial \overleftrightarrow{\mathbf{G}}}{\partial y}(\mathbf{r}_0, \mathbf{r}_0, \omega) = \frac{-1}{8\pi^2\varepsilon_0\varepsilon_1} \iint k_y \overleftrightarrow{\mathbf{M}} e^{i2k_{z1}h} dk_x dk_y. \quad (A21)$$

Writing the transverse wave vector components in cylindrical coordinates $k_x = k_t\cos\phi$, $k_y = k_t\sin\phi$, and $dk_x dk_y = k_t dk_t d\phi$ and performing the angular integration in ϕ we arrive at a single integration for the Green function derivatives:

$$\frac{\partial \overleftrightarrow{\mathbf{G}}}{\partial x}(\mathbf{r}_0, \mathbf{r}_0, \omega) = \frac{1}{8\pi\varepsilon_0\varepsilon_1} \int dk_t e^{i2k_{z1}h} k_t^3$$
$$\times \begin{pmatrix} 0 & 0 & r_{pp} \\ 0 & 0 & r_{sp}k_1/k_{z1} \\ -r_{pp} & r_{ps}k_1/k_{z1} & 0 \end{pmatrix}, \quad (A22)$$

$$\frac{\partial \overleftrightarrow{\mathbf{G}}}{\partial y}(\mathbf{r}_0, \mathbf{r}_0, \omega) = \frac{1}{8\pi\varepsilon_0\varepsilon_1} \int dk_t e^{i2k_{z1}h} k_t^3$$
$$\times \begin{pmatrix} 0 & 0 & -r_{sp}k_1/k_{z1} \\ 0 & 0 & r_{pp} \\ -r_{ps}k_1/k_{z1} & -r_{pp} & 0 \end{pmatrix}. \quad (A23)$$

The angular integration in ϕ shown here is only valid when the Fresnel reflection coefficients are rotationally symmetric (i.e., r_{pp}, r_{ss}, r_{sp}, and r_{ps} are independent of ϕ) as is the case in our current geometry. Care should be taken if considering other surfaces, where this rotational symmetry might be broken.

APPENDIX B: TIME-AVERAGED FORCE ON A DIPOLE NEAR A SURFACE WITH CROSS-POLARIZED REFLECTION

The time-averaged optical force $\langle\mathbf{F}\rangle$ acting on the dipole is given by [41,43,44]

$$\langle\mathbf{F}\rangle = \sum_{i=x,y,z} \frac{1}{2}\text{Re}\{p_i^*\nabla E_i\}, \quad (B1)$$

where ∇ is the gradient with respect to $\mathbf{r}$ evaluated at $\mathbf{r}_0$, and $\mathbf{E} = (E_x, E_y, E_z)$ is the field reflected by the surface, acting

back on the dipole, which can be written using the Green's function approach as seen in Eq. (A17). Replacing this into Eq. (B1), we arrive at

$$\langle \mathbf{F} \rangle = \sum_{i,j=x,y,z} \frac{1}{2} \text{Re} \left\{ p_i^* p_j \left(\frac{\partial G_{ij}}{\partial x} \hat{\mathbf{x}} + \frac{\partial G_{ij}}{\partial y} \hat{\mathbf{y}} + \frac{\partial G_{ij}}{\partial z} \hat{\mathbf{z}} \right) \right\}.$$

(B2)

Here we are interested on the lateral force components, which are given by

$$\langle F_x \rangle = \sum_{i,j=x,y,z} \frac{1}{2} \text{Re} \left\{ p_i^* p_j \frac{\partial G_{ij}}{\partial x} \right\},$$

(B3)

$$\langle F_y \rangle = \sum_{i,j=x,y,z} \frac{1}{2} \text{Re} \left\{ p_i^* p_j \frac{\partial G_{ij}}{\partial y} \right\}.$$

(B4)

1. Force over *x* axis

Performing the summation over each element of the tensor defined in Eq. (A22), we obtain the optical force over the *x* axis as

$$\langle F_x \rangle = \frac{1}{2} \text{Re} \left\{ p_x^* p_z \frac{\partial G_{xz}}{\partial x} + p_z^* p_x \frac{\partial G_{zx}}{\partial x} + p_y^* p_z \frac{\partial G_{yz}}{\partial x} + p_z^* p_y \frac{\partial G_{zy}}{\partial x} \right\},$$

(B5)

where we can substitute the terms from the Green function tensor from Eq. (A22). In the case of materials with off-diagonal permittivity components as considered here, it turns out that the cross-polarization Fresnel reflection coefficients $r_{sp} = r_{ps}$ are identical to each other [60,61], allowing us to rewrite Eq. (B5) in the following way:

$$\langle F_x \rangle = \frac{1}{2} \text{Re} \left\{ \frac{1}{8\pi \varepsilon_0 \varepsilon_1} \int dk_t e^{i2k_{z1}h} k_t^3 \left[r_{pp}(p_x^* p_z - p_z^* p_x) + \frac{k_1}{k_{z1}} r_{ps}(p_y^* p_z + p_z^* p_y) \right] \right\}.$$

(B6)

This is an exact expression in terms of all of the variables of the system and could be given as a final equation. However, we can gain some further insight by performing substitutions, with the aim of writing the dipole components in terms of the degree of circular and diagonal polarization, and to write the force in terms of the Kerr rotation. To this end, substituting $2i\text{Im}[p_x^* p_z] = p_x^* p_z - p_z^* p_x$, $2\text{Re}[p_y^* p_z] = p_y^* p_z + p_z^* p_y$ and the Kerr rotation $\Phi_K = r_{ps}/r_{pp}$ into Eq. (B6) we get

$$\langle F_x \rangle = \frac{1}{2} \text{Re} \left\{ \frac{1}{8\pi \varepsilon_0 \varepsilon_1} \int dk_t e^{i2k_{z1}h} k_t^3 r_{pp} \times \left[2i\text{Im}\{p_x^* p_z\} + \frac{k_1}{k_{z1}} 2\text{Re}\{p_y^* p_z\} \Phi_K \right] \right\}.$$

(B7)

It is now very convenient to introduce the power radiated by the dipole as a measure of its amplitude [16]. The power radiated by a dipole **p** in a medium with permittivity $\varepsilon_0 \varepsilon_1$ and refractive index n_1 can be written as the sum of the power radiated by each of its components. The power radiated by only two of those components *i* and *j* (where *i*, *j* = *x*, *y*, or *z*)

in free space is given by

$$P_{\text{rad}}^{ij} = \frac{c_0 k_0^4 n_1^3}{12\pi \varepsilon_0 \varepsilon_1} (|p_i|^2 + |p_j|^2).$$

(B8)

Using the above definition, we can rewrite Eq. (B7) as

$$\langle F_x \rangle = \frac{3}{4c_0 k_0^4 n_1^3} \text{Re} \left\{ \int dk_t e^{i2k_{z1}h} k_t^3 r_{pp} \left[i \frac{2\text{Im}\{p_x^* p_z\}}{|p_x|^2 + |p_z|^2} P_{\text{rad}}^{xz} + \frac{k_1}{k_{z1}} \frac{2\text{Re}\{p_y^* p_z\}}{|p_y|^2 + |p_z|^2} P_{\text{rad}}^{yz} \Phi_K \right] \right\},$$

(B9)

now we can introduce convenient symbols which describe the polarization of our dipole. For example, the "spin" of the dipole particle around the *y* axis can be defined as $\sigma_y = -\frac{2\text{Im}[p_x^* p_z]}{|p_x|^2 + |p_z|^2}$, while $\chi^{yz} = \frac{2\text{Re}[p_y^* p_z]}{|p_y|^2 + |p_z|^2}$ can be used as a measure of the degree of diagonal polarization on the *yz* plane. It will be maximum when the dipole is linearly polarized at 45° to the surface normal. Both σ_y and χ^{yz} closely resemble the expressions of Stokes parameters. Substituting these measures, we get

$$\langle F_x \rangle = \frac{-3}{4c_0 k_0^4 n_1^3} \text{Re} \left\{ \int dk_t e^{i2k_{z1}h} k_t^3 r_{pp} \times \left[i\sigma_y P_{\text{rad}}^{xz} - \frac{k_1}{k_{z1}} \chi^{yz} \Phi_K P_{\text{rad}}^{yz} \right] \right\},$$

(B10)

This equation is completely general for any dipole polarization.

2. Force over *y* axis

We can perform the analogous steps to calculate the force along the *y* axis. The result is, evidently, identical to that of the force along the *x* axis, but with the dipole components suitably rotated:

$$\langle F_y \rangle = \frac{-3}{4c_0 k_0^4 n_1^3} \text{Re} \left\{ \int dk_t e^{i2k_{z1}h} k_t^3 r_{pp} \times \left[-i\sigma_x P_{\text{rad}}^{yz} + \frac{k_1}{k_{z1}} \chi^{xz} \Phi_K P_{\text{rad}}^{xz} \right] \right\},$$

(B11)

where the spin of the dipole particle around the *x* axis has been defined as $\sigma_x = \frac{2\text{Im}[p_y^* p_z]}{|p_y|^2 + |p_z|^2}$, and $\chi^{xz} = \frac{2\text{Re}[p_x^* p_z]}{|p_x|^2 + |p_z|^2}$ is the degree of diagonal polarization on the *xz* plane.

3. Further simplifications

The first term in the integrand of Eq. (B11) is the well-known recoil force for circularly polarized dipoles over a surface [16–19]. However, the second term explicitly depends on the magneto-optical response and corresponds to novel physics. In order to isolate this term and study its behavior, we may consider a polarized particle $\mathbf{p} = [p_x, 0, p_z]$ on the *xz* plane. The lateral optical force in the *y* direction is then simplified to

$$\langle F_y \rangle = \frac{-3\chi^{xz}}{4c_0 k_0^4 n_1^3} P_{\text{rad}}^{xz} \text{Re} \left\{ \int dk_t e^{i2k_{z1}h} k_t^3 r_{pp} \frac{k_1}{k_{z1}} \Phi_K \right\}.$$

(B12)

Now we can introduce the normalized transverse wave-vector $k_{\text{tr}} = k_t/k_0$ to normalize the integrals above defined. This change allows us to write $dk_t = k_0 \, dk_{\text{tr}}$, $k_{z1} =$

$k_0\sqrt{\varepsilon_1 - k_{\mathrm{tr}}^2}$, and $k_0 = \omega/c_0 = 2\pi/\lambda$. This normalization is very convenient because we arrive at an expression of the force as a function that is independent of frequency except for the effect of the normalized height (h/λ), and is proportional to the power radiated by the dipole. This expression therefore becomes very general for any frequency and dipole:

$$\langle F_y \rangle = -\frac{3}{4c_0 n_1^2} \chi^{xz} P_{\mathrm{rad}}^{xz}$$
$$\times \mathrm{Re}\left\{ \int_0^\infty r_{pp} e^{4i\pi\left(\frac{h}{\lambda}\right)\sqrt{\varepsilon_1^2 - k_{\mathrm{tr}}^2}} k_{\mathrm{tr}}^3 \frac{\Phi_K}{\sqrt{\varepsilon_1^2 - k_{\mathrm{tr}}^2}} dk_{\mathrm{tr}} \right\},$$
(B13)

which reduces to Eq. (2) when $\varepsilon_1 = n_1 = 1$.

APPENDIX C: FRESNEL REFLECTION COEFFICIENTS FOR AN MO SURFACE WHEN THE MAGNETIZATION IS ALONG THE Z AXIS

We consider the structure shown in Fig. 5, which consists of an interface between isotropic (ε_1) and MO ($\overset{\leftrightarrow}{\varepsilon_2}$) material. We have considered the magnetization of the MO material along the negative z axis. Then, the corresponding permittivity tensor can be written as

$$\overset{\leftrightarrow}{\varepsilon_2} = \begin{pmatrix} \varepsilon_{xx} & \varepsilon_{xy} & 0 \\ \varepsilon_{yx} & \varepsilon_{yy} & 0 \\ 0 & 0 & \varepsilon_{zz} \end{pmatrix},$$
(C1)

where $\varepsilon_{xx} = \varepsilon_{yy} = \varepsilon_{zz} = \varepsilon_2$ and $\varepsilon_{yx} = -\varepsilon_{xy}$.

To describe the propagation of the electromagnetic waves through both the isotropic and the MO material, we have obtained the z component of the wave vector and the proper polarization modes in each medium by solving the corresponding wave equation [34,35]. The expression of these wave vectors are shown below:

$$k_{z1} = k_0\sqrt{\varepsilon_1 - k_{\mathrm{tr}}^2} = k_0 N_{z1},$$
(C2)

$$k_{z21} = k_0\sqrt{N_{z2}^2 + i\frac{\varepsilon_{xy}}{\sqrt{\varepsilon_2}}N_{z2}} = k_0 N_{z21},$$
(C3)

$$k_{z23} = k_0\sqrt{N_{z2}^2 - i\frac{\varepsilon_{xy}}{\sqrt{\varepsilon_2}}N_{z2}} = k_0 N_{z23},$$
(C4)

with $k_0 = \omega/c$, $k_{\mathrm{tr}} = k_t/k_0$, and $N_{z2} = \sqrt{\varepsilon_2 - k_{\mathrm{tr}}^2}$ (which would correspond to the case when the medium 2 does not have a MO response). From a computational point of view,
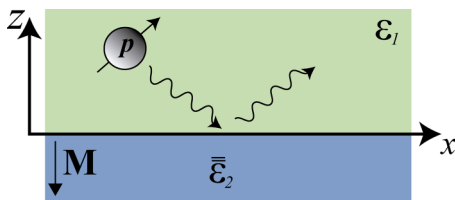

FIG. 5. Schematic representation of the system under study, ε_1 and $\overset{\leftrightarrow}{\varepsilon_2}$ are the corresponding dielectric permittivity and dielectric permittivity tensor for isotropic incident medium and magneto-optical material, respectively.

it is very important to use the correct sign when doing the square root for the various N_z's. Calculations must use the sign which results in a positive imaginary part (or positive real part if purely real). After obtaining the associated normal modes in each medium and implementing the boundary conditions at the interface, a system of equations can be solved to arrive at the Fresnel reflection coefficients at the interface, which are written as [34,35]

$$r_{pp} = -\frac{A_{pp}}{B},$$
(C5)

$$r_{ss} = \frac{A_{ss}}{B},$$
(C6)

$$r_{ps} = \frac{A_{ps}}{B},$$
(C7)

where

$$A_{pp} = \varepsilon_1 N_{z2}^2 (2N_{z1} + N_{z21} + N_{z23})$$
$$- N_{z1}[2N_{z21}N_{z23} + N_{z1}(N_{z21} + N_{z23})]\varepsilon_2,$$
(C8)

$$A_{ss} = \varepsilon_1 N_{z2}^2 (2N_{z1} - N_{z21} - N_{z23})$$
$$+ N_{z1}[-2N_{z21}N_{z23} + N_{z1}(N_{z21} + N_{z23})]\varepsilon_2,$$
(C9)

$$A_{ps} = -2iN_{z1}N_{z2}(N_{z21} - N_{z23})\sqrt{\varepsilon_1}\sqrt{\varepsilon_2},$$
(C10)

$$B = \varepsilon_1 N_{z2}^2 (2N_{z1} + N_{z21} + N_{z23})$$
$$+ N_{z1}[2N_{z21}N_{z23} + N_{z1}(N_{z21} + N_{z23})]\varepsilon_2.$$
(C11)

APPENDIX D: APPROXIMATIONS ON THE FORCE: QUASISTATIC AND FIRST-ORDER APPROXIMATIONS

We can apply the near-field quasistatic approximation with the intention to obtain simpler expressions that allow us to better understand the origin of the force. This approximation is valid when the dipole is very close to the substrate—the case under study—where the lateral force of interest to this work is strongest. We assume $k_t \gg k_0$ implying that we can take the limit $k_t/k_0 \to \infty$ and the Fresnel reflection coefficients r_{ps} and the MO Kerr rotation ($\Phi_K = r_{ps}/r_{pp}$) are written in the quasistatic limit as

$$r_{pp}^{\mathrm{QS}} = \frac{\varepsilon_2 - \varepsilon_1}{\varepsilon_2 + \varepsilon_1},$$
(D1)

$$r_{ps}^{\mathrm{QS}} = \frac{-i\sqrt{\varepsilon_1}\varepsilon_{xy}}{2(\varepsilon_1 + \varepsilon_2)k_{\mathrm{tr}}},$$
(D2)

$$\Phi_K^{\mathrm{QS}} = \frac{-i\sqrt{\varepsilon_1}\varepsilon_{xy}}{2(\varepsilon_2 - \varepsilon_1)k_{\mathrm{tr}}}.$$
(D3)

Substituting the previous results into the expression of the lateral force (B13) allows one to solve the integration analytically to obtain the near-field approximation:

$$\langle F_y^{\mathrm{QS}} \rangle = \frac{3\chi^{xz}}{128c_0\pi^2 n_1^2} P_{\mathrm{rad}}^{xz} \mathrm{Re}\left\{ \frac{\sqrt{\varepsilon_1}\varepsilon_{xy}}{(\varepsilon_1 + \varepsilon_2)} \right\} \left(\frac{h}{\lambda} \right)^{-2},$$
(D4)

which reduces to Eq. (3) when $\varepsilon_1 = n_1 = 1$.

Alternatively, we can also derive a first-order approximation of the force, with the assumption that the off-diagonal component of the permittivity is small, while not neglecting phase retardation. We will rewrite the reflection coefficients
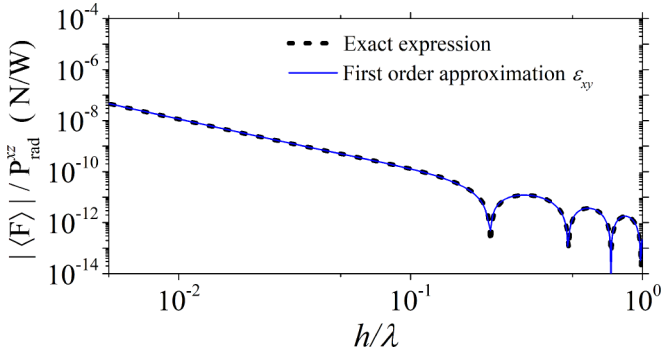
FIG. 6. Distance dependence of the time-averaged lateral forces over a linearly polarized dipole $\mathbf{p} = (1, 0, 1)$, located above a realistic magneto-optical surface (diagonal $\varepsilon_2 = -10.51 + 2.10i$ and off-diagonal $\varepsilon_{xy} = -1.20 + 1.15i$ element of the permittivity tensor). The exact expression of $\langle F_y \rangle$ is depicted by a dashed line, while the approximation to first order in ε_{xy} is depicted by a solid line.

expressed in Eqs. (C5)–(C7) in a simpler way by considering only first-order (linear) corrections due to the off-diagonal permittivity component ε_{xy}. These simplified reflection coefficients can then be introduced into Eq. (B13) to calculate the approximate lateral force. We check the validity of this simplified form by comparing the exact and approximate forms and find excellent agreement.

First, we assume that the off-diagonal elements in the permittivity tensor of a magnetized medium are much smaller than the diagonal ones, $\varepsilon_{xy} \ll \varepsilon_2$. In this case we can expand the reflection coefficients to first order in ε_{xy}, as seen below:

$$r_{pp}^{\text{Approx}} = \frac{N_{z1}\varepsilon_2 - N_{z2}\varepsilon_1}{N_{z1}\varepsilon_2 + N_{z2}\varepsilon_1}, \tag{D5}$$

$$r_{ps}^{\text{Approx}} = \frac{n_1 N_{z1}\varepsilon_{xy}}{(N_{z1} + N_{z2})(N_{z1}\varepsilon_2 + N_{z2}\varepsilon_1)}, \tag{D6}$$

$$\Phi_K^{\text{Approx}} = \frac{n_1 N_{z1}\varepsilon_{xy}}{(N_{z1} + N_{z2})(N_{z1}\varepsilon_2 - N_{z2}\varepsilon_1)}. \tag{D7}$$

With this approximation, the lateral force can be expressed as

$$\langle F_y \rangle^{\text{Approx}} = -\frac{3}{4c_0 n_1^2} \chi^{xz} P_{\text{rad}}^{xz}$$

$$\times \text{Re}\left\{ \int_0^\infty \frac{r_{ps}^{\text{Approx}}}{N_{z1}} e^{4i\pi\left(\frac{h}{\lambda}\right)N_{z1}} k_{\text{tr}}^3 dk_{\text{tr}} \right\}. \tag{D8}$$

In Fig. 6 we calculate the exact expression of the lateral force acting on a linearly polarized dipole and compare it with the first order one, Eq. (D8). We see that the approximated expression allows us to reliably describe the obtained results, and also allows any reader to simplify, in a considerable way, the calculation time of the integrals.

APPENDIX E: DIFFERENT CONTRIBUTIONS TO THE LATERAL FORCE

The integrand in the force in Eq. (2) has several distinct features which we can consider separately. For added physical insight, it is highly convenient to decompose the integrand

into three separate contributions, as proposed in Ref. [16]:

$$\langle F_y \rangle = \langle F_y^{\text{QS}} \rangle + \langle F_y^{\text{pw}} \rangle + \langle F_y^{\text{recoil}} \rangle. \tag{E1}$$

The first term is the quasistatic approximation, which corresponds to the integrand at very high values of k_{tr}, and is calculated in Appendix D [Eq. (D4)]. This term varies like h^{-2} and hence dominates the force when $h \to 0$, in the very near field.

The second term is the force caused by the propagating plane waves, radiated by the dipole, reflected on the surface, and acting back on the dipole. This force is very weak for practical purposes but has long range, and therefore it always dominates at sufficiently high distances. It dominates above approximately $h \approx \lambda/2\pi$. Mathematically, this term can be calculated by limiting the integral in Eq. (2) to the far-field region $0 \leqslant k_{\text{tr}} \leqslant 1$ only:

$$\langle F_y^{\text{pw}} \rangle = -\frac{3}{4c_0} P_{\text{rad}}^{xz} \chi$$

$$\times \text{Re}\left\{ \int_0^1 r_{pp} e^{4i\pi\left(\frac{h}{\lambda}\right)\sqrt{1-k_{\text{tr}}^2}} k_{\text{tr}}^3 \frac{\Phi_K}{\sqrt{1-k_{\text{tr}}^2}} dk_{\text{tr}} \right\}. \tag{E2}$$

Due to the complex exponential, which represents the phase propagation of the waves, this term of the force oscillates in sign with increasing distance, which is seen in the log-log plot as periodic inverted peaks going to zero. The sign of this term flips every $\lambda/4$ increase in height h, because the total increase in propagation distance for the plane waves is equal to $2h$, due to the round trip from the dipole to the surface and back again.

The third term is the contribution to the force due to the mode recoil, and is the most difficult to calculate. This term is associated with the existence of complex poles in the Fresnel reflection coefficient $r_{ps}(k_{\text{tr}})$ when we consider k_{tr} as a complex variable. Each complex pole in the reflection coefficient represents a distinct mode in the surface or system of slabs. When the modes have low loss, the poles are close to the real line, and appear as distinct sharp peaks in the integrand of Eq. (2). In that case (low losses) it is very easy to estimate the contribution of the peak to the integral by approximating the peak via a delta function $\text{Im}\{r_{ps}(k_{\text{tr}})\} \approx R\delta(k_{\text{tr}} - n_{\text{eff}})$ where $n_{\text{eff}} > 1$ is the effective mode index, and hence integrating Eq. (2) over the delta function:

$$\langle F_y^{\text{recoil}} \rangle \approx \frac{-3P_{\text{rad}}^{xz}\chi}{4c_0} \frac{Rn_{\text{eff}}^3}{\sqrt{n_{\text{eff}}^2 - 1}} e^{-4\pi\sqrt{n_{\text{eff}}^2-1}\left(\frac{h}{\lambda}\right)}, \tag{E3}$$

where R is a measure of the mode excitation efficiency, and can be estimated via the integration of the peak using a suitable bandwidth Δ that embraces the whole resonant peak $R = \int_{n_{\text{eff}}-\Delta/2}^{n_{\text{eff}}+\Delta/2} \text{Im}\{r_{ps}(k_{\text{tr}})\} dk_{\text{tr}}$. Notice that this term of the force decays exponentially with height, as one would expect for a mode recoil force due to the evanescent tails of the mode. This term turns out to be negligible in some of the force plots presented in the paper, but sometimes dominates at intermediate near-field distances, between the region of quasistatic force and the region of propagating plane wave force.

The appropriateness of dividing the force into these three terms, each with a very distinct behavior, is clearly observed
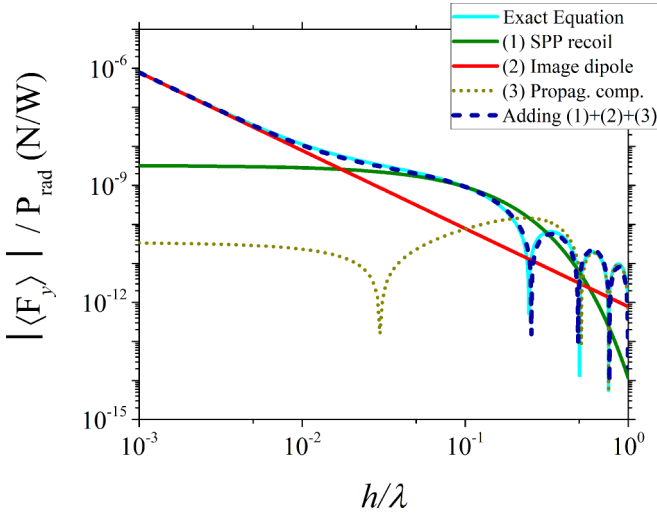
FIG. 7. Distance dependence of the time-averaged lateral forces over a linearly polarized dipole $\mathbf{p} = (1, 0, 1)$, located above a magneto-optical substrate (diagonal $\varepsilon_2 = -2 + 0.1i$ and off-diagonal $\varepsilon_{xy} = -i$ element of the permittivity tensor). The exact result from Eq. (2) and the different terms in the approximation are shown. For the calculation of R_k we used $\Delta_k = 0.56$ and $n_{eff} = 1.41$. The material was chosen to show the three terms as clearly as possible.

in Fig. 7, which shows the distance h/λ dependence of the total force on a material system, calculated exactly via Eq. (2) together with the contribution from the three different terms, each with its own distance dependence. Notice how the quasistatic term dominates for $h < 0.01\lambda$, the mode recoil (in this case SPPs) term dominates for $0.01\lambda < h < 0.2\lambda$, and the propagating plane wave term dominates for $h > 0.2\lambda$. The three terms add up together to account for the exact force. Performing this decomposition in very lossy materials such as the realistic materials considered in the main text is not straightforward because the calculation of the recoil mode contribution is difficult to estimate when the peak in the integrand is very broad.

APPENDIX F: CALCULATION OF THE SURFACE PLASMON POLARITON'S ELECTRIC FIELD IN A SINGLE MO INTERFACE

We briefly describe here our general approach to determine the dispersion relation and the electric field of the surface electromagnetic modes in our MO interface. These results are of great importance to calculate the radiation diagram discussed in Eq. (4). Assuming that the interface is located at $z = 0$, as in Fig. 8, the electric field of the surface mode can be written in each medium as

$$\mathbf{E}_r = (E_s^+ \hat{\mathbf{e}}_s + E_p^+ \hat{\mathbf{e}}_p^+) e^{i(\mathbf{k}_r \cdot \mathbf{r} - \omega t)}, \quad z > 0,$$

$$\mathbf{E}_t = (\mathbf{E}_1 + \mathbf{E}_3) e^{i(\mathbf{k}_t \cdot \mathbf{r} - \omega t)}, \quad z < 0. \quad \text{(F1)}$$

The electric field vectors $\mathbf{E}_1$ and $\mathbf{E}_3$ correspond to eigenmodes of the wave equation inside the MO material. The amplitudes of the $\mathbf{E}_1$ and $\mathbf{E}_3$ components can be expressed in terms of the x components, that is, $E_{yj} = p_j E_{xj}$ and $E_{zj} =$

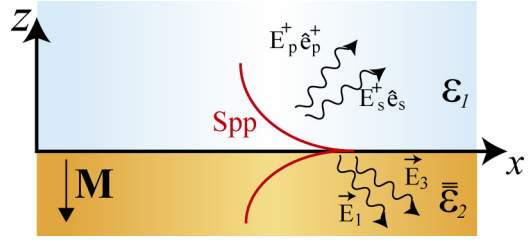

FIG. 8. Schematic diagram of a plasmonic excitation on a single-MO interface.

$q_j E_{xj}$. This allows us to write the transmitted field as [35]

$$\mathbf{E}_1 = (E_{x1}, E_{y1}, E_{z1}) = E_{x1}(1, p_1, q_1),$$

$$\mathbf{E}_3 = (E_{x3}, E_{y3}, E_{z3}) = E_{x3}(1, p_3, q_3), \quad \text{(F2)}$$

with $p_j = \frac{\varepsilon_{xy}}{N_2^2 - N_{z2j}^2}$, $q_j = \frac{n_{SPP} N_{z2j}}{N_{z2}^2}$ and the normalized transverse wave vector $k_{tr} = k_t/k_0 = n_{SPP}$ is equal to the plasmon mode effective index.

The requirements of the continuity for the electric and magnetic field components parallel to the interface plane $z = 0$ provide four equations, which can be written in matrix form as

$$\begin{pmatrix} -1 & 0 & p_1 & p_3 \\ N_{z1} & 0 & N_{z21} p_1 & N_{z23} p_3 \\ 0 & -N_{z1}/N_1 & 1 & 1 \\ 0 & N_1 & N_{z21} + q_1 n_{spp} N_{z23} + q_3 n_{spp} \end{pmatrix}$$

$$\times \begin{pmatrix} E_s^+ \\ E_p^+ \\ E_{x1} \\ E_{x3} \end{pmatrix} = \begin{pmatrix} 0 \\ 0 \\ 0 \\ 0 \end{pmatrix}. \quad \text{(F3)}$$

Nontrivial solutions to this system correspond to the surface modes at the interface, and exist only when the determinant of the matrix is equal to zero. After some algebra, the determinant of the matrix can be written as

$$N_{z1}[2N_{z21}N_{z23} + N_{z1}(N_{z21} + N_{z23})]\varepsilon_2$$

$$+ n_1^2 N_{z2}^2(2N_{z1} + N_{z21} + N_{z23}) = 0. \quad \text{(F4)}$$

The solution of Eq. (F4) provides the explicit values of the transverse wave vector ($k_0 n_{SPP}$) for the plasmonic excitation, which must be calculated numerically. Once n_{SPP} is known, we can calculate the coefficients for the fields of this surface mode by solving Eq. (F3). We can express the field coefficients in terms of E_{x1} as seen below:

$$\frac{E_s^+}{E_{x1}} = \frac{(N_{z23} - N_{z21})}{(N_{z2}^2 - N_{z21}^2)(N_{z1} + N_{z23})} \varepsilon_{xy}, \quad \text{(F5)}$$

$$\frac{E_p^+}{E_{x1}} = \frac{n_1(N_{z23} - N_{z21})[N_{z2}^2 + N_{z21}N_{z23} + N_{z1}(N_{z21} + N_{z23})]}{N_{z1}(N_{z1} + N_{z23})(N_{z2}^2 - N_{z21}^2)}.$$

$$\text{(F6)}$$

Finally, we can obtain the ratio of s to p polarization of the surface mode, which is an important parameter for understanding the existence of this new lateral force. After

some algebra, this ratio is expressed as

$$\alpha = \frac{E_s^+}{E_p^+} = \frac{N_{z1}\varepsilon_{xy}}{n_1\left[N_{z2}^2 + N_{z21}N_{z23} + N_{z1}(N_{z21} + N_{z23})\right]}. \quad \text{(F7)}$$

APPENDIX G: NET MOMENTUM CARRIED BY THE EXCITED SURFACE PLASMONS

Substituting the plasmon radiation diagram Eq. (4) into the angular integration of the vector momentum of each excited plasmon mode Eq. (5), we can analytically evaluate the integration and arrive at

$$\begin{pmatrix} \mathcal{P}_x \\ \mathcal{P}_y \end{pmatrix} \propto 2\pi \begin{pmatrix} \text{Im}[p_x p_z^* n_{\text{SPP}} \sqrt{n_{\text{SPP}}^2 - 1}] \\ \text{Re}[p_x p_z^* n_{\text{SPP}} \alpha] \end{pmatrix}. \quad \text{(G1)}$$

When the surface is lossless, then n_{SPP}, $\sqrt{n_{\text{SPP}}^2 - 1}$, and α are all real, leading to the expression in the main text.

APPENDIX H: COMPARISON OF NOVEL LATERAL FORCE WITH PREVIOUSLY KNOWN LATERAL FORCES

In order to put this novel lateral force into context, we provide here a direct comparison with the known circular dipole's lateral force, both over the MO Co_6Ag_{94} substrate from Fig. 2 and a bulk gold surface [62], as used in Ref. [16]. For these examples, $\mathbf{p}^{\text{diag}} = (1, 0, 1)$, $\mathbf{p}^{\text{circ}} = (1, 0, i)$, and the
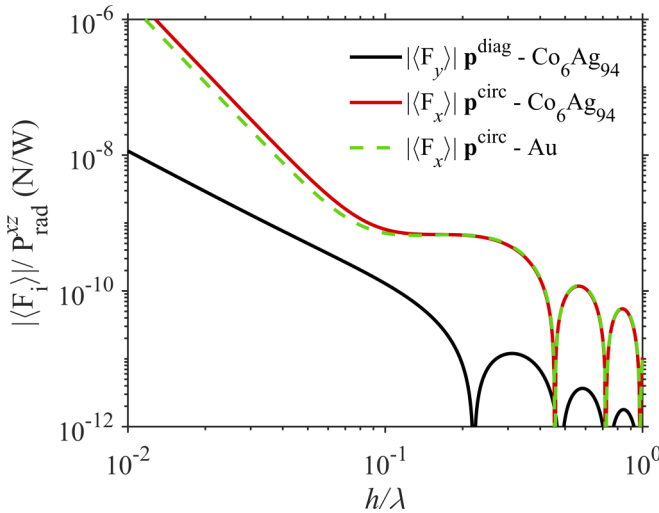

FIG. 9. The lateral forces of diagonal and circular dipoles over MO (Co_6Ag_{94} with a magnetic field of 0.8 T) and non-magneto-optical (Au) substrates, normalized by the scattering power.
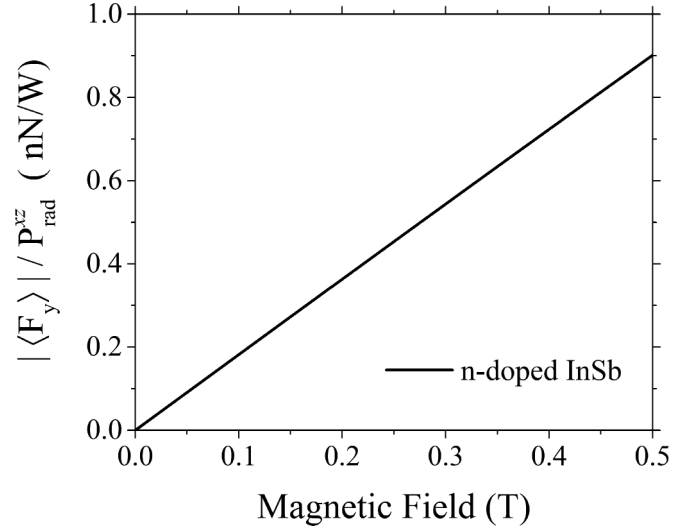

FIG. 10. Magnetic field dependence of the time-averaged lateral forces over a linearly polarized dipole $\mathbf{p} = (1, 0, 1)$, located above an n-doped InSb substrate. The dipole is located at $h = 0.01\lambda$ and its angular frequency is $\omega = 3.6 \times 10^{13}$ rad/s. The elements of the permittivity tensor of InSb follow the model reported in Refs. [63,64] taking into account that, for low values of magnetic field, the difference between the diagonal elements of the permittivity tensor can be safely neglected.

dipoles radiate at 631 nm. In Fig. 9, we compare the $|\langle F_y \rangle|$ of $\mathbf{p}^{\text{diag}}$ against the $|\langle F_x \rangle|$ of $\mathbf{p}^{\text{circ}}$.

For these particular materials, the circular dipole experiences a greater lateral force than an equally powerful diagonal dipole. Of course, the MO force can be increased by increasing the material magnetization, which could make the forces comparable. With smaller distances, the circular dipole will always overcome the diagonal dipole eventually, thanks to its h^{-4} height dependence, compared to h^{-2} for the MO based diagonal dipole.

We emphasize that in all scenarios, these forces are proportional to the scattering power of the dipole and so increasing the power always provides a theoretical avenue for enhancing optical forces.

To demonstrate the effect of changing the magnetic field, in Fig. 10 we show the magnetic field dependence of the time-averaged lateral forces acting on a linearly polarized dipole $\mathbf{p} = (1, 0, 1)$, located above a n-doped InSb substrate. The elements of permittivity tensor for InSb were taken following the analytical model of Refs. [63,64], allowing us to test different values of the magnetic field. The figure shows the linear growth of the force with the magnetic field, as expected, because the nondiagonal element ε_{xy} depends linearly with the magnetic field at low values of magnetic field [see Eq. (3)].

[1] R. Loudon and C. Baxter, Proc. R. Soc. London Ser. A **468**, 1825 (2012).

[2] L. Allen, S. M. Barnett, and M. J. Padgett, *Optical Angular Momentum* (IOP, London, 2003).

[3] S. Chu, Rev. Mod. Phys. **70**, 685 (1998).

[4] W. D. Phillips, Rev. Mod. Phys. **70**, 721 (1998).

[5] A. Ashkin, Phys. Rev. Lett. **24**, 156 (1970).

[6] A. Ashkin and J. M. Dziedzic, Appl. Phys. Lett. **19**, 283 (1971).

[7] A. Ashkin, J. M. Dziedzic, J. E. Bjorkholm, and S. Chu, Opt. Lett. **11**, 288 (1986).

[8] V. S. Bagnato, G. P. Lafyatis, A. G. Martin, E. L. Raab, R. N. Ahmad-Bitar, and D. E. Pritchard, Phys. Rev. Lett. **58**, 2194 (1987).

[9] A. Ashkin, IEEE J. Sel. Top. Quantum Electron. **6**, 841 (2000).

[10] D. G. Grier, Nature (London) **424**, 810 (2003).

[11] M. Aspelmeyer, T. J. Kippenberg, and F. Marquardt, Rev. Mod. Phys. **86**, 1391 (2014).

[12] F. J. Rodríguez-Fortuño, G. Marino, P. Ginzburg, D. O'Connor, A. Martínez, G. A. Wurtz, and A. V. Zayats, Science **340**, 328 (2013).

[13] J. Petersen, J. Volz, and A. Rauschenbeutel, Science **346**, 67 (2014).

[14] D. O'Connor, P. Ginzburg, F. J. Rodríguez-Fortuño, G. A. Wurtz, and A. V. Zayats, Nat. Commun. **5**, 5327 (2014).

[15] K. Y. Bliokh, F. J. Rodríguez-Fortuño, F. Nori, and A. V. Zayats, Nat. Photon. **9**, 796 (2015).

[16] F. J. Rodríguez-Fortuño, N. Engheta, A. Martínez, and A. V. Zayats, Nat. Commun. **6**, 8799 (2015).

[17] S. B. Wang and C. T. Chan, Nat. Commun. **5**, 3307 (2014).

[18] S. Sukhov, V. Kajorndejnukul, R. R. Naraghi, and A. Dogariu, Nat. Photon. **9**, 809 (2015).

[19] A. Hayat, J. P. B. Mueller, and F. Capasso, Proc. Natl. Acad. Sci. USA **112**, 13190 (2015).

[20] A. Manjavacas, F. J. Rodríguez-Fortuño, F. Javier García de Abajo, and A. V. Zayats, Phys. Rev. Lett. **118**, 133605 (2017).

[21] S. A. H. Gangaraj, G. W. Hanson, M. G. Silveirinha, K. Shastri, M. Antezza, and F. Monticone, Phys. Rev. B **99**, 245414 (2019).

[22] S. A. H. Gangaraj and F. Monticone, IEEE Antennas Wireless Propag. Lett. **17**, 1993 (2018).

[23] S. A. H. Gangaraj and G. W. Hanson, IEEE Antennas Wireless Propag. Lett. **16**, 449 (2017).

[24] S. Ali Hassani Gangaraj and F. Monticone, J. Phys.: Condens. Matter **30**, 104002 (2018).

[25] M. G. Silveirinha, S. A. H. Gangaraj, G. W. Hanson, and M. Antezza, Phys. Rev. A **97**, 022509 (2018).

[26] S. A. Hassani Gangaraj, G. W. Hanson, M. Antezza, and M. G. Silveirinha, Phys. Rev. B **97**, 201108(R) (2018).

[27] N. Rotenberg, M. Spasenović, T. L. Krijger, B. le Feber, F. J. García de Abajo, and L. Kuipers, Phys. Rev. Lett. **108**, 127402 (2012).

[28] I. S. Sinev, A. A. Bogdanov, F. E. Komissarenko, K. S. Frizyuk, M. I. Petrov, I. S. Mukhin, S. V. Makarov, A. K. Samusev, A. V. Lavrinenko, and I. V. Iorsh, Laser Photon. Rev. **11**, 1700168 (2017).

[29] S.-Y. Lee, I.-M. Lee, J. Park, S. Oh, W. Lee, K.-Y. Kim, and B. Lee, Phys. Rev. Lett. **108**, 213907 (2012).

[30] A. B. Evlyukhin and S. I. Bozhevolnyi, Phys. Rev. B **92**, 245419 (2015).

[31] M. Neugebauer, P. Woźniak, A. Bag, G. Leuchs, and P. Banzer, Nat. Commun. **7**, 11286 (2016).

[32] M. F. Picardi, A. V. Zayats, and F. J. Rodríguez-Fortuño, Phys. Rev. Lett. **120**, 117402 (2018).

[33] J. J. Kingsley-Smith, M. F. Picardi, L. Wei, A. V. Zayats, and F. J. Rodríguez-Fortuño, Phys. Rev. B **99**, 235410 (2019).

[34] P. Yeh, Surf. Sci. **96**, 41 (1980).

[35] S. Visnovsky, *Optics in Magnetic Multilayers and Nanostructures* (CRC Taylor & Francis, London, 2006).

[36] G. Armelles, A. Cebollada, A. García-Martín, and M. U. González, Adv. Opt. Mater. **1**, 10 (2013).

[37] L. E. Kreilkamp, V. I. Belotelov, J. Y. Chin, S. Neutzner, D. Dregely, T. Wehlus, I. A. Akimov, M. Bayer, B. Stritzker, and H. Giessen, Phys. Rev. X **3**, 041019 (2013).

[38] M. Inoue, M. Levy, and A. V. Baryshev, *Magnetophotonics: From Theory to Applications* (Springer, Berlin, 2013).

[39] L. Mandel and E. Wolf, *Optical Coherence and Quantum Optics* (Cambridge University Press, Cambridge, 1995).

[40] M. Nieto-Vesperinas, *Scattering and Diffraction in Physical Optics* (World Scientific, Singapore, 2006).

[41] L. Novotny and B. Hecht, *Principles of Nano-optics* (Cambridge University Press, Cambridge, 2012), p. 564.

[42] M. F. Picardi, A. Manjavacas, A. V. Zayats, and F. J. Rodríguez-Fortuño, Phys. Rev. B **95**, 245416 (2017).

[43] J. P. Gordon and A. Ashkin, Phys. Rev. A **21**, 1606 (1980).

[44] P. C. Chaumet and M. Nieto-Vesperinas, Opt. Lett. **25**, 1065 (2000).

[45] F. J. Rodríguez-Fortuño, A. Vakil, and N. Engheta, Phys. Rev. Lett. **112**, 033902 (2014).

[46] W.-M. Zheng, S.-Y. Wang, D.-L. Qian, Y.-X. Zheng, Y.-M. Yang, B.-Y. Li, and L.-Y. Chen, J. Magn. Magn. Mater. **198-199**, 210 (1999).

[47] S.-Y. Wang, W.-M. Zheng, D.-L. Qian, R.-J. Zhang, Y.-X. Zheng, S.-M. Zhou, Y.-M. Yang, B.-Y. Li, and L.-Y. Chen, J. Appl. Phys. **85**, 5121 (1999).

[48] P. Johnson and R. Christy, Phys. Rev. B **9**, 5056 (1974).

[49] Š. Višňovský, R. Krishnan, M. Nývlt, and V. Prosser, J. Magn. Soc. Jpn. **20**, Suppl. S1, 41 (1996).

[50] Š. Višňovský, K. Postava, T. Yamaguchi, and R. Lopusnik, Appl. Opt. **41**, 3950 (2002).

[51] T. Van Mechelen and Z. Jacob, Optica **3**, 118 (2016).

[52] I. J. Luxmoore, N. A. Wasley, A. J. Ramsay, A. C. T. Thijssen, R. Oulton, M. Hugues, S. Kasture, V. G. Achanta, A. M. Fox, and M. S. Skolnick, Phys. Rev. Lett. **110**, 037402 (2013).

[53] L. Marrucci, Nat. Phys. **11**, 9 (2015).

[54] B. le Feber, N. Rotenberg, and L. Kuipers, Nat. Commun. **6**, 6695 (2015).

[55] R. J. Coles, D. M. Price, J. E. Dixon, B. Royall, E. Clarke, P. Kok, M. S. Skolnick, A. M. Fox, and M. N. Makhonin, Nat. Commun. **7**, 11183 (2016).

[56] A. Espinosa-Soria and A. Martinez, IEEE Photon. Technol. Lett. **28**, 1561 (2016).

[57] A. Aiello, P. Banzer, M. Neugebauer, and G. Leuchs, Nat. Photon. **9**, 789 (2015).

[58] I. Sinev, A. Bogdanov, F. Komissarenko, I. Mukhin, A. Samusev, I. Iorsh, and A. Lavrinenko, J. Phys.: Conf. Ser. **1092**, 012140 (2018).

[59] N. K. Paul, D. Correas-Serrano, and J. S. Gomez-Diaz, Phys. Rev. B **99**, 121408(R) (2019).

[60] M. Mansuripur, *Classical Optics and Its Applications* (Cambridge University Press, Cambridge, 2012), p. 713.

[61] V. Protopopov, *Practical Opto-Electronics. An Illustrated Guide for the Laboratory* (Springer International, New York, 2014), p. 401.

[62] E. D. Palik, *Handbook of Optical Constants of Solids* (Academic, San Diego, 1998).

[63] E. D. Palik, R. Kaplan, R. W. Gammon, H. Kaplan, R. F. Wallis, and J. J. Quinn, Phys. Rev. B **13**, 2497 (1976).

[64] E. Moncada-Villa, V. Fernández-Hurtado, F. J. García-Vidal, A. García-Martín, and J. C. Cuevas, Phys. Rev. B **92**, 125418 (2015).